Mn_3O_4(001) film growth on Ag(001) - a systematic study using NEXAFS, STM, and LEED

K. Gillmeister, M. Huth, R. Shantyr, M. Trautmann, K. Meinel, A. Chassé, K.-M. Schindler, and H. Neddermeyer

Institut für Physik, Martin-Luther-Universität Halle-Wittenberg, Halle, Germany

W. F. Widdra

Institut für Physik, Martin-Luther-Universität Halle-Wittenberg, Halle, Germany and

Max-Planck-Institut für Mikrostrukturphysik, Halle, Germany

(Dated: August 11, 2016)

Abstract

The film growth of Mn_3O_4(001) films on Ag(001) up to film thicknesses of almost seven unit cells of Mn_3O_4 has been monitored using a complementary combination of near-edge X-ray absorption fine structure spectroscopy (NEXAFS), scanning tunneling microscopy (STM), and low-energy electron diffraction (LEED). The oxide films have been prepared by molecular beam epitaxy. Using NEXAFS, the identity of the Mn oxide has clearly been determined as Mn_3O_4. For the initial stages of growth, oxide islands with p(2×1) and p(2×2) structures are formed, which are embedded into the substrate. For Mn_3O_4 coverages up to 1.5 unit cells a p(2×1) structure of the films is visible in STM and LEED. Further increase of the thickness leads to a phase transition of the oxide films resulting in an additional c(2×2) structure with a 45° rotated atomic pattern. The emerging film structures are discussed on the basis of a sublayer model of the Mn_3O_4 spinel unit cell. While the polarity of the island edges determines the structure of initial islands, the surface energy of thicker layers is remarkably reduced by a film restructuring.

I. INTRODUCTION

Building up on the seminal investigations of oxide films of NiO[1] and CoO[2], manganese oxide (MnO) films have been grown and investigated on Pt(111)[3–6], Pd(001)[7–10], Ru(001)[11], Rh(111)[12], and Ag(001)[13–17]. A common feature of all these film systems is that the rock salt unit cells of these materials have only one sort of atomic sublayer in the (001)-plane. Here, we focus on Hausmannit (Mn_3O_4) a spinel with a stack of 8 sublayers and a Jahn-Teller distortion of the unit cell in c direction. All its simple bulk terminations in the (001)-plane are polar, which makes it particularly interesting to study the layer-by-layer build up of Mn_3O_4 films.

So far, only the growth of $Mn_3O_4(110)$ on $SrTiO_3(110)$[18] and the growth of $Mn_3O_4(001)$ on MnO(001)[19] are reported. For $Mn_3O_4(001)$/MnO(001), electron diffraction showed that the $Mn_3O_4(001)$ films grow parallel to $\langle 110 \rangle$ directions of the underlying MnO(001) lattice. This means that the $(a_{Mn_3O_4} \times a_{Mn_3O_4})$ unit mesh is rotated by 45° resulting in a (2×2) LEED pattern with respect to the MnO(001) substrate. Such a 45° rotation has also been observed for other film - substrate combinations ,e.g., LiF, KCl, and NaI on MgO(001)[20] and NaCl on Ag(001)[21]. According to the 'roles of lattice fitting in epitaxy'[20], a 45° rotated orientation has to be expected if the ratio $a_{film} : a_{substrate}$ of the lattice parameters is close to $\sqrt{2}$. For the 45° rotated growth of $Mn_3O_4(001)$ on Ag(001) ($a_{Ag} = 409$ pm, $a_{Mn_3O_4} = 576$ pm) one obtains an almost vanishing misfit of 0.3% (Fig. 1). Consequently, one can expect a perfect film structure when growing $Mn_3O_4(001)$ films on Ag(001) compared to MnO(001) films on this substrate.

In the present study, Mn_3O_4 films have been prepared on Ag(001) by means of reactive Mn deposition in O_2 atmosphere[22]. Structure, morphology, composition, and electronic properties of the films have been characterized using low-energy electron diffraction (LEED), scanning tunneling microscopy (STM), Auger electron spectroscopy (AES), and near edge X-ray absorption fine structure spectroscopy (NEXAFS). Starting from the initial island stage up to thicknesses of several Mn_3O_4 unit cells (height: 946 pm), the development of the surface structure as a function of film thickness and annealing is reported.

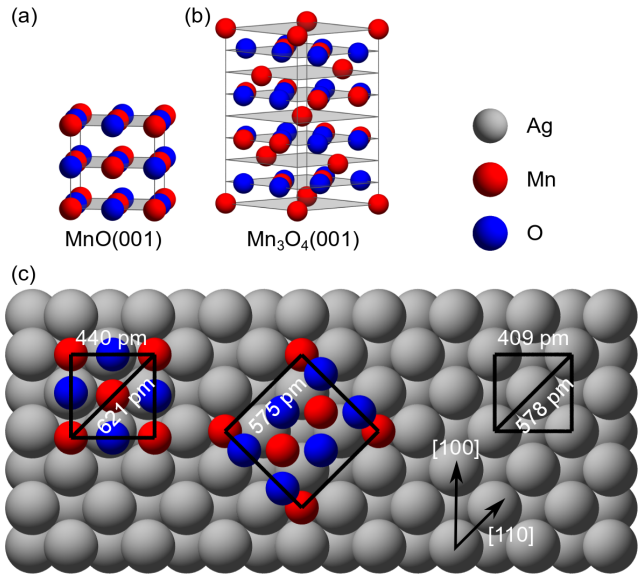

FIG. 1. Hard sphere models of unit cells of (a) rock salt MnO(001) and (b) spinel $Mn_3O_4(001)$ on Ag(001). (c) Lattice fittings for MnO(001)/Ag(001) (lattice misfit 7.6%) and 45° rotated Mn_3O_4/Ag(001) (lattice mismatch 0.3%).

II. EXPERIMENTAL

Experiments have been performed in three different ultra-high vacuum (UHV) systems. The first is equipped with an STM, a spot profile analysis (SPA)-LEED optics, and a cylindrical mirror analyzer (CMA) for Auger electron spectroscopy (AES). The second system contains a conventional LEED optic and a low-temperature STM, operating at 100 K. The base pressures of both chambers are in the low 10^{-10} mbar range. In addition, a third UHV chamber equipped with a LEED optics has been used for NEXAFS studies recorded at the beamline UE56-2 PGM-2 (energy range: 100-1000 eV) at the synchrotron radiation facility BESSY II[23]. Spectra were recorded in total electron yield mode. Normalization to the incident X-ray flux was achieved according to the photo current from the last refocusing mirror of the beamline. All presented LEED patterns have been recorded with the SPA-LEED optics.

The Ag(001) crystals (miscut $< 0.2°$) were cleaned by cycles of Ar^+ ion sputtering (600 V, 2 μA) at room temperature and subsequent heating at 630 K until they showed a clean, defect free surface in STM and sharp spots in the LEED pattern. Manganese was evaporated from Ta crucibles heated by electron bombardment. The deposition rate of 30 pm (i.e. 0.03 ML)

per minute was calibrated by means of a quartz microbalance, AES, LEED, and STM and controlled by monitoring the flux of Mn ions as reported previously[5]. The deposition was performed at sample temperatures between room temperature and 450 K.

The integral structure of the as grown Mn_3O_4 films was characterized by LEED. The local film morphology was investigated by STM in constant current mode. The equivalence of films obtained in the different UHV systems was checked using LEED.

III. RESULTS

A. NEXAFS of MnO and Mn_3O_4

Manganese can occur in various oxidation states. In our case, the particular Mn oxidation state is determined by the oxygen partial pressure and substrate temperature during growth. At low oxygen partial pressures MnO with Mn^{2+} should be formed. With increasing pressure, a transition to the formation of the next higher oxide Mn_3O_4 with a mix of Mn^{2+} and Mn^{3+} is expected. In the following, LEED and NEXAFS are used to identify the films prepared at different oxygen partial pressures. MnO(001) films on Ag(001) with a thickness of 4 ML have been obtained by reactive evaporation of Mn in 5×10^{-8} mbar O_2 with the Ag(001) substrate at room temperature. Annealing the film results in brilliant and sharp LEED spots showing the (1×1) pattern of strained MnO(001) as reported previously[17,24]. Assuming pseudomorphic growth of the MnO film on the Ag(100) substrate, 4 ML MnO equal to 48.0 Mn ions/nm^2.

NEXAFS spectra at the O K absorption edge are depicted in Fig. 2a. The spectra agree with published spectra of MnO films grown on Ag(001)[15] and are characteristic for MnO(001). They show only minor differences between normal (0°) and grazing light incidence (70° off-normal). This indicates only minor deviations from a cubic bulk-like structure of MnO (Fig. 1). In the bulk structure, the octahedral coordination of the Mn ions by six O ions leads to an isotropic environment and no NEXAFS dependencies on angle of light incidence or polarization. In ultrathin films, however, MnO growths strained due to the lattice mismatch between Ag and MnO. For a thickness of 4 ML the film is not yet relaxed to the bulk structure, but exhibits a lateral compression and a corresponding vertical expansion[24]. The resulting lowering of the symmetry from cubic to tetragonal might explain the small

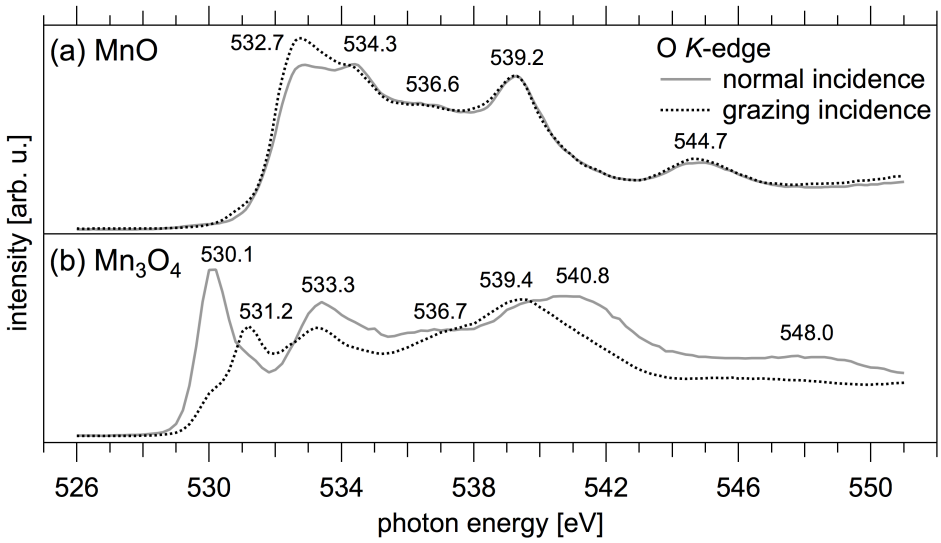

FIG. 2. NEXAFS spectra of (a) 4 ML MnO and (b) 20 MLE Mn_3O_4 on Ag(001) for normal and grazing X-ray incidence. For a detailed discussion see the text.

differences in Fig. 2 at 533 eV. In addition, the reduced coordination of Mn ions in the top surface layer and in the bottom layer at the interface to the Ag substrate can contribute to this anisotropy.

In order to obtain the oxygen richer Mn_3O_4 films, the O_2 pressure during Mn evaporation was increased systematically. At an O_2 pressure of 5×10^{-7} mbar, a change in the LEED pattern and the NEXAFS spectra is observed. The LEED spots become sharp and brilliant again. Depending on film thickness, a $p(2 \times 1)$ or an apparent (2×2) superstructure relative to the Ag(001) substrate develops. The latter is composed of $p(2 \times 1)$ and $c(2 \times 2)$ domains, as will be shown later. The superstructures observed correspond to a pseudomorphic Mn_3O_4 film rotated by 45° around the surface normal as visualized schematically in Fig. 1.

The corresponding NEXAFS spectra for a $Mn_3O_4(001)$ film with a thickness equivalent to 20 monolayers (MLE, 1 MLE $\hat{=}$ 12 Mn ions/nm^2) at the O K-edge in Fig. 2b are very similar to those of bulk Mn_3O_4[25]. The film thickness is given in terms of the equivalent amount of Mn ions, which makes the comparison of different phases easier. The bulk crystal structure of Mn_3O_4 has a unit cell height of 947,0 pm consists of 8 sublayers. A unit cell high Mn_3O_4 film corresponds to 36 Mn ions/nm^2. The Mn_3O_4 film of fig. 2, therefore, has a thickness of 6.7 unit cells or about 50 sublayers. The NEXAFS spectrum of the Mn_3O_4 film shows 7 resonances at 530.1 eV, 531.2 eV, 533.3 eV, 536.7 eV, 539.4 eV, 540.8, and 548.0

eV. The energies of all resonances agree well with resonances in electron loss fine structure spectra at the O K-edge of Mn_3O_4[26,27]. The presence of α-Mn_2O_3 can clearly be ruled out, since its characteristic resonance at 542 eV is missing in 2b. Instead, the two resonances at 539.4 and 540.8 eV and the one at 548 eV are characteristic for Mn_3O_4 and not present at all in α-Mn_2O_3. However, the spectra of γ-Mn_2O_3 and Mn_3O_4 are very similar and can hardly be distinguished[28]. This similarity originates in nearly identical geometric structures with no difference in bond lengths and angles. The only difference is the occupation of octahedral and tetrahedral sites by Mn ions and γ-Mn_2O_3 can be considered as a vacancy structure of Mn_3O_4, whereby the occupation of octahedral or tetrahedral sites has not fully been resolved. Investigations in the late 50's arrived at controversial results (tetrahedral vacancies by Goodenough et al.[29] and octahedral vacancies by Sinha et al.[30]) which have not been further investigated later on. Our subsequent discussion will be based on the vacancy-less structure of Mn_3O_4, because we started from growth conditions for MnO and slowly increased the oxygen pressure. Mn_3O_4 is expected to be formed prior to Mn_2O_3 due to its lower oxygen content.

Compared to the NEXAFS spectra of MnO, the absorption onset in the Mn_3O_4 spectra is shifted characteristically to a lower photon energy. Since this edge is very prominent, its absence in the first spectrum clearly rules out even small amounts of Mn_3O_4 in the MnO film.

Contrary to MnO, the NEXAFS spectra of the Mn_3O_4 film strongly depend on the angle of light incidence. Taking into account that the bulk structure of Mn_3O_4 has a tetragonal unit cell (Fig. 1) with different atomic arrangements of O ions around Mn ions, the dependence of the x-ray absorption on the angle of incidence indicates directly a c-axis alignment of the Mn_3O_4(001) film. Since the shorter a axis of Mn_3O_4 matches better to the lattice of the substrate, preferential alignment of the c-axis normal to the surface is assumed.

B. Initial stages of film formation

The initial stages of film growth for Mn_3O_4 on Ag(001) at a substrate temperature of 450 K have been characterized by STM. After the deposition of 0.1 nm Mn_3O_4, two different island types can be distinguished in STM images as shown in Fig. 3(a). One type of islands is of rectangular shape and has a well-resolved striped atomic pattern pointing along [110]

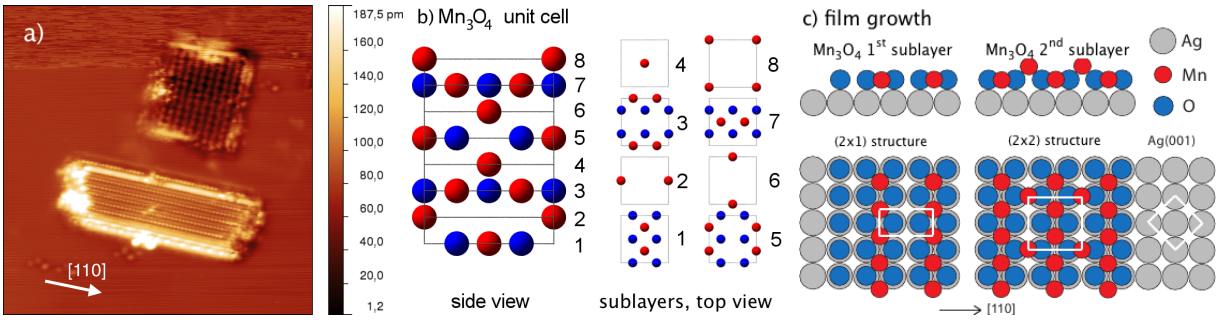

FIG. 3. (a) STM image (20×20 nm^2, -0.2 V, 0.7 nA) of a 0.1 nm thick Mn_3O_4 film on Ag(001) with a quadratic (top) and a rectangular (bottom) island, (b) sphere model of the Mn_3O_4 unit cell and its 8 sublayers, (c) film growth on Ag(001) for the first and second sublayers.

directions. The other type of islands appears darker, i.e. has a lower apparent height and a quadratic atomic pattern with edges along [110] directions. For the interpretation of the STM images we start with hard sphere models of the bulk $Mn_3O_4(001)$ unit cell as depicted in Fig. 3b. Any Jahn-Teller distortion is neglected here as well as later. The bulk structure of $Mn_3O_4(001)$ is composed of two types of layers (sublayers), both with a square (a $\times$ a) unit cell (Fig. 3b). One layer is a mixed oxygen/manganese layer with Mn_2O_4 composition (layers 1, 3, 5, 7). The other layer is manganese only (layers 2, 4, 6, 8). These layers are stacked alternatingly whereby consecutive layers of the same type are laterally displaced by a/2 and rotated by 90°. Eight layers form the complete unit cell with an overall height of c = 947 pm.

The layered stacking scheme of the $Mn_3O_4(001)$ unit cell readily hints to possible interface structures of $Mn_3O_4(001)$ on Ag(001) in (see Fig. 3c). The square (a $\times$ a) unit cell is assumed to be arranged along [110] directions of the Ag(001) substrate. As mentioned above this orientation leads to a nearly perfect lattice match between the $Mn_3O_4(001)$ layer and the Ag(001) substrate. In Fig. 3c, a Mn_2O_4 sublayer (layer 1) is assumed as the interface layer of the film. Oxygen ions are located at top positions of the Ag atoms, whereas manganese ions reside in fourfold hollow sites, as found with CoO on Ag(100)[31]. On top of this mixed manganese/oxygen interface layer, the manganese ions of the second sublayer (layer 2) are in bridge positions above two oxygen ions. According to this scheme, the Mn ions in the mixed manganese/oxygen correspond to octahedrally coordinated Mn of the bulk and form a p(2 $\times$ 1) structure. The Mn ions of the manganese only layer correspond to the tetrahedrally

coordinated Mn in the bulk and form a p(2 × 2) structure.[32] These two structures fit well to the two different Mn_3O_4 islands at the initial stage of growth as found by STM in Fig. 3a. The quadratic atomic pattern of the top island is aligned along [110] directions and corresponds to the p(2 × 2) structure whereas the bottom island displays the characteristic rows of the p(2 × 1) structure running along $\langle 110 \rangle$ or $\langle 1\bar{1}0 \rangle$. As the nominal film thickness is one tenth of a unit cell, one can assume that the local thickness of the bottom p(2 × 1) island is just one sublayer and that of the top p(2 × 2) island is two sublayers.

Interestingly, the p(2 × 1) islands prefer a rectangular shape with the long sides parallel to Mn (2 × 1) rows. On the contrary, the p(2 × 2) islands grow in a nearly quadratic shape. Obviously, edge energies or diffusion barriers of the p(2×1) islands differ strongly along $\langle 110 \rangle$ and $\langle 1\bar{1}0 \rangle$. This can actually be related to the atomic structures according to Fig. 3c. Along the Mn (2 × 1) rows the island edges are formed by a couple of complete Mn and O rows, respectively. In the perpendicular direction every second Mn ion is missing in the Mn rows. Although both edge types are polar, the polarity of edges parallel to the Mn (2 × 1) rows could be smaller due to a better balance of ionic charges. In the case of the p(2 × 2) islands, the difference in polarity might be smaller due to the additional top Mn ions in the vicinity of the island edges. Hence, island shapes close to quadratic are favored. Islands with polar edge orientations that are immersed into the substrate have also been observed for other rock system with rock salt structure, like CoO/Ag(001)[33], NiO/Ag(001)[34], MnO/Ag(001), and MgO/Ag(001)[35]. There, the polar edge orientations have been found to be stabilized by island immersion into the Ag substrate, which is enabled by the facile diffusion of Ag even at room temperature. Similar immersion effects are also expected for Mn_3O_4(001) islands of Fig. 3 , in line with the presence of polar edges.

C. Thin films of 6 and 12 sublayers

Figures 4 a and d show STM images obtained after the deposition of 6 and 12 sublayers of Mn_3O_4 on Ag(001). After deposition at room temperature the film was annealed to 630 K to increase film quality. The STM image in Fig. 4a shows Mn_3O_4 islands with p(2 × 1) stripes surrounded by flat Ag areas. Whereas the nominal thickness is 6 sublayers, the Mn_3O_4 islands cover only 70% of the image. Therefore, the local island thickness must be considerably larger. Different step heights can be found in the line profile of Fig. 4b. A

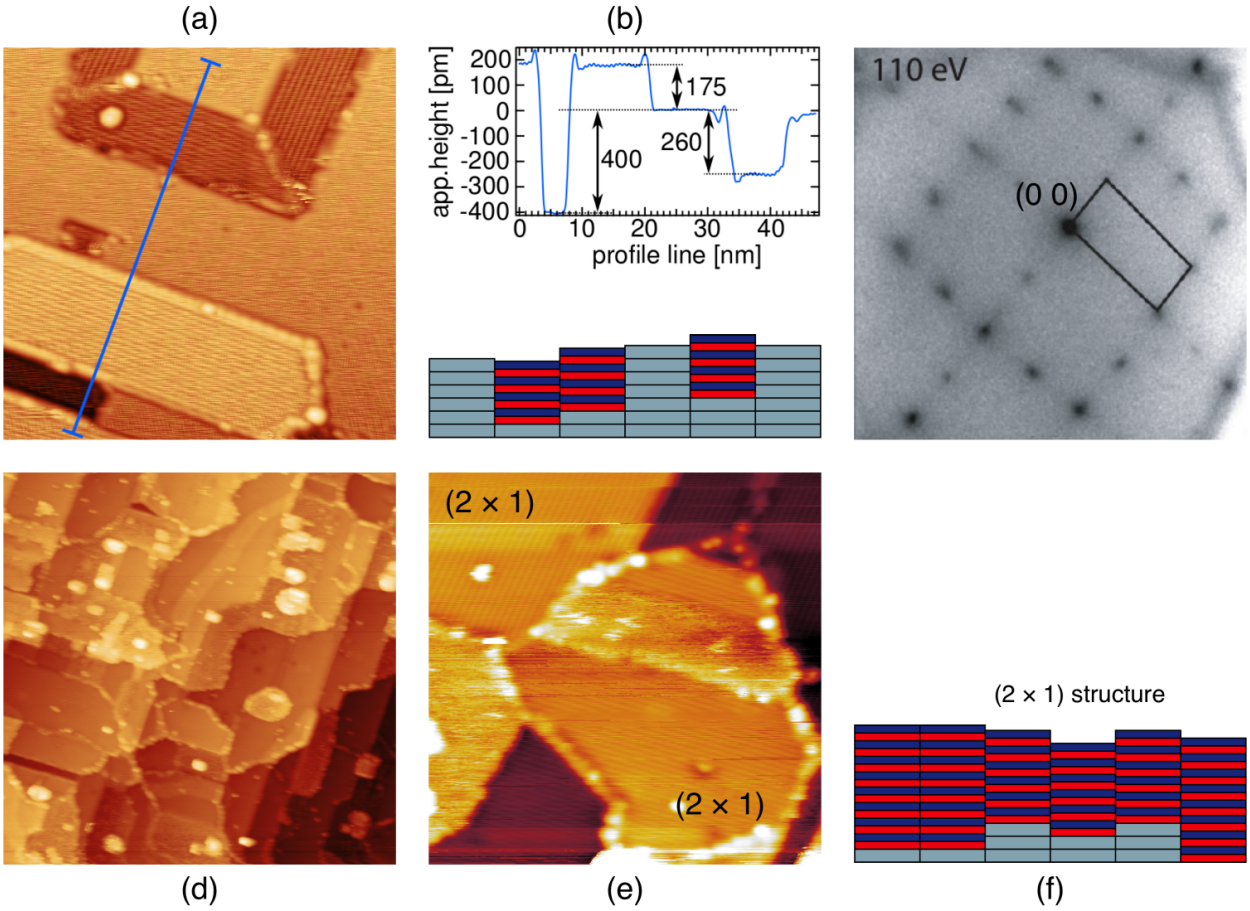

FIG. 4. (a) STM image of a 6 sublayer Mn_3O_4 film on Ag(001) (46 × 46 nm^2, 2.0 V, 0.8 nA) (b) height profile along the blue line; (c) LEED pattern of the oxide films of 6 sublayers with a p(2 × 1) unit cell. (d) STM image of a 12 sublayer film Mn_3O_4 on Ag(001) (120 × 120 nm^2, 1.3 V, 0.8 nA) (e) zoomed-in STM image (36 × 36 nm^2, 2.0 V, 0.5 nA); (f) scheme of the 12 sublayer film on the silver substrate.

height of 400 pm fits that of the Ag(001) unit cell (a_{Ag}: 409 pm). The other values of 260 and 175 pm, respectively, could result from Mn_3O_4 islands that are embedded into the silver substrate as indicated by the scheme of Fig. 4b. Due to different local thicknesses and/or depths of embedding, islands appear with different contrasts. However, no clear conclusion about this fact is possible since the electronic structure of the Mn_3O_4 islands needs to be taken into account when determining heights from STM images[33]. Exactly as at low coverage, the p(2 × 1) islands prefer a rectangular shape with long edges running along the MnO (2 × 1) rows (compare to Fig. 3). The same islands are also observed but rotated by 90°, which is actually expected from the fourfold symmetry of the Ag(001)

substrate. Where such islands meet, they form domain boundaries along [100] directions. Contrary to the initial stages p(2×2) structures like the ones in Fig. 3 a have not been found for the 6 sublayer film. The surface termination of these p(2×2) structures is with Mn ions only and theoretical investigations[19] have shown that for an Mn_3O_4 film with a thickness >8 sublayers the energy of this termination is significantly higher than that of an Mn_2O_4 termination with its p(2×1) structure. The LEED pattern shown in Fig. 4c gives informations about the integral structure of the prepared sample. One can recognize a p(2×1) superstructure with two domains that are rotated by 90°. In agreement to the STM images, no spots of a p(2×2) superstructure have been found at any electron energy. The LEED pattern of the film of 12 sublayers has been found to be identical to the 6 sublayer one.

D. Thin films of more than 15 sublayers

After the deposition of 15 sublayers of Mn_3O_4 at room temperature and subsequent annealing to 630 K one can distinguish five different structures in the STM image of Fig. 5a. The flat regions F show the same stripe p(2×1) superstructure like the islands found for 12 sublayers. Additionally, stripe-like (4×1) structures (S) and atomically resolved c(2×2) structures (C) were found. The wide stripes of the (4×1) superstructure are exactly twice as wide as those of the (2×1) structure. The $\times 1$ periodicity along the (4×1) stripes is not resolved here. Atomic models of the structures are depicted in Fig. 6. Starting point is the Mn_2O_4 top layer from Fig. 3c. The proposal for the (4×1) superstructure with wide stripes is obtained by moving every second Mn row in the [110] direction towards a neighboring row (Fig. 6b). The c(2×2) structure is obtained by moving every second ion of an Mn row of the p(2×1) structure along the [110] direction to the neighboring fourfold hollow site. The resulting atomic pattern is rotated by 45° with respect to the p(2×1) structure and the island edges become non-polar (Fig. 6c).

The regions S with the striped (4×1) superstructure in Fig. 5a are much smaller than the other ones. Therefore, they do not result in additional spots in the LEED pattern. On the other hand, the number of islands with a c(2×2) structure is large enough to lead to additional spots in the diffraction pattern as is seen in Fig. 6d. The LEED pattern in Fig. 6d could result from two different structural arrangements. The first one is a

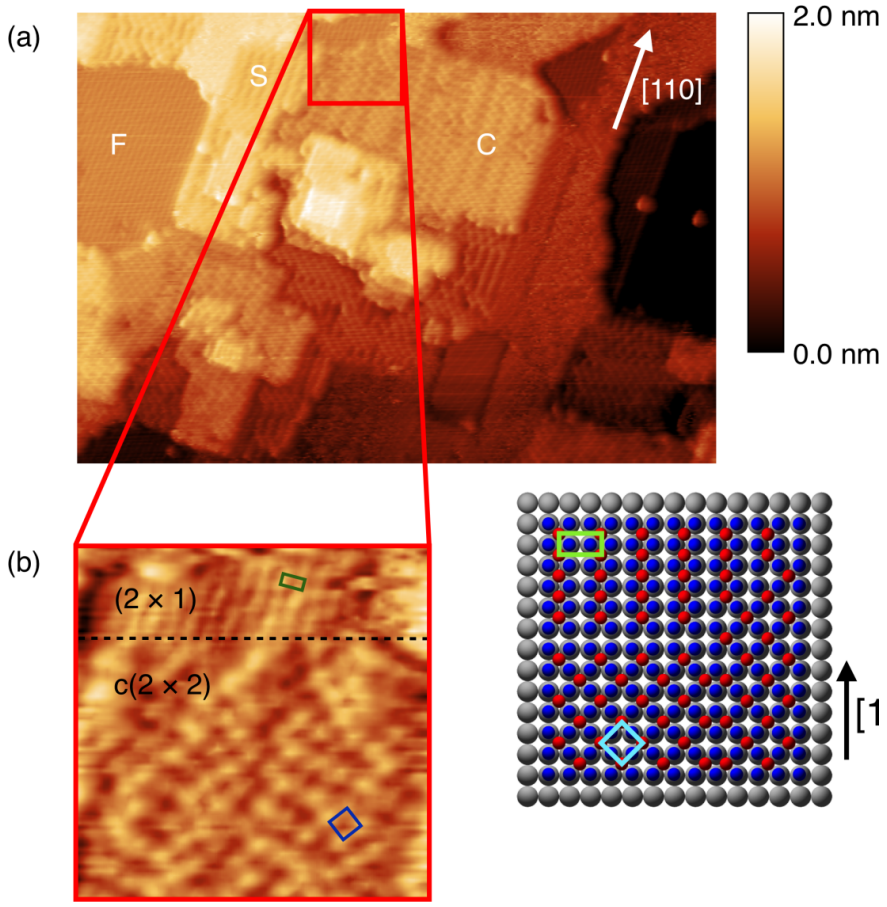

FIG. 5. (a) STM image of a 15 sublayers Mn_3O_4 film on Ag(001) (58 × 47 nm^2, 2.0 V, 0.3 nA). The capital letters mark different structures at the surface; (b) STM detail (11×11 nm^2, FFT filtered) of (a) together with the atomic model visualizing the phase transition from a p(2 × 1) to a c(2 × 2) structure. For further details see the text.

p(2 × 2) superstructure as found for the initial stages (Fig. 3a). The second one is a combination of p(2 × 1) and c(2 × 2) superstructures (see Fig. 6d). Again, the p(2 × 2) superstructure is excluded because of the substantially higher surface energy of the pure Mn termination[19]. Furthermore, the model with a mix of p(2 × 1) and c(2 × 2) superstructures is supported by the STM images. It is also supported by the fact that both the p(2 × 1) and c(2 × 2) superstructures correspond to a coverage of 0.5, which makes their coexistence and the transition from one to the other very easy, whereas a p(2 × 2) superstructure usually corresponds to a coverage of 0.25 or 0.75. Therefore, transitions between the p(2 × 1) and the p(2 × 2) superstructure would require considerable mass transport across the surface.

The coexistence of the p(2 × 1) and c(2 × 2) structures can nicely be seen in Fig. 5b.

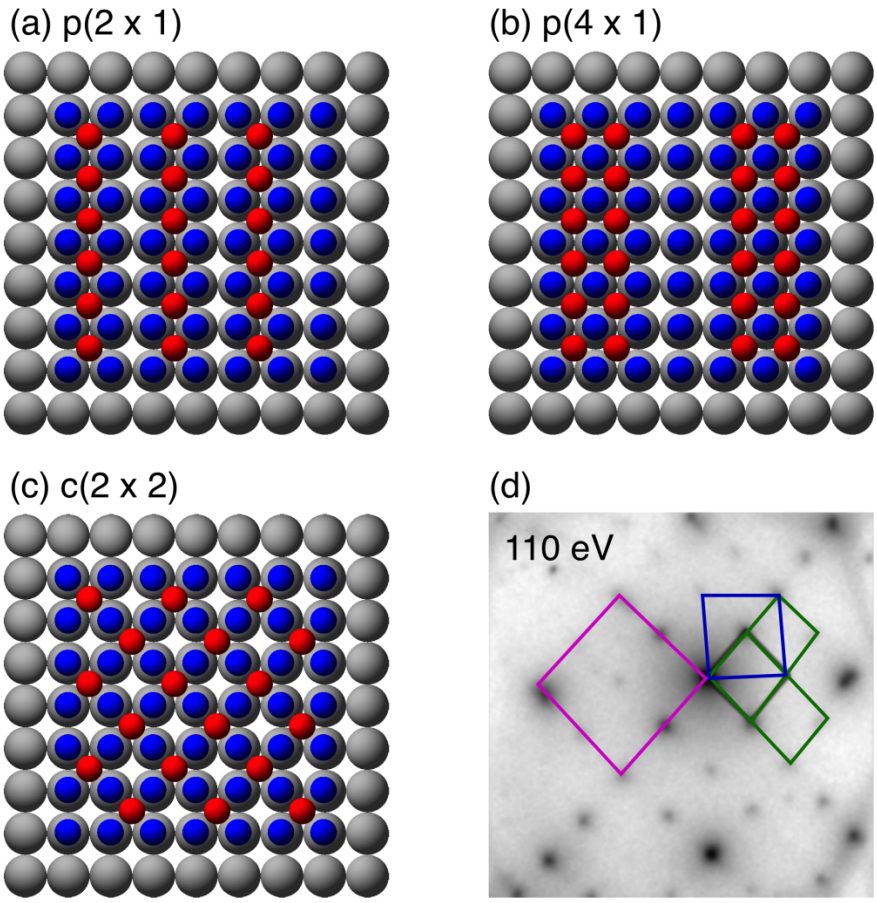

FIG. 6. (a) p(2 × 1), (b) p(4 × 1) and (c) c(2 × 2) Mn_2O_4 superstructures on Ag(001) and (d) LEED pattern at 110 eV for the 15 sublayer Mn_3O_4 film on Ag(001) including unit cells of the p(2 × 1) (green), c(2 × 2) (blue), and p(2 × 2) (magenta) superstructures.

One can recognize the p(2 × 1) rows in the upper part of the image and in the atomic model next to the image. At a certain point, marked with the dashed black line, the rows begin to break down and the Mn ions are rearranged. The zigzag pattern of the c(2 × 2) mesh is visible in the model as well as in the STM image. Also, the rotation of the c(2 × 2) pattern by 45° becomes obvious.

The coexistence of p(2×1) and c(2×2) structures instead of a simple p(2×2) structure can also be underpinned by the following consideration. The p(2×1) and c(2×2) superstructures correspond to a coverage of 0.5, which makes their coexistence and the transition from one to the other very easy, whereas a p(2 × 2) superstructure usually corresponds to a coverage of 0.25 or 0.75. Therefore, transitions between the p(2 × 1) and the p(2 × 2) superstructure would require considerable mass transport across the surface.

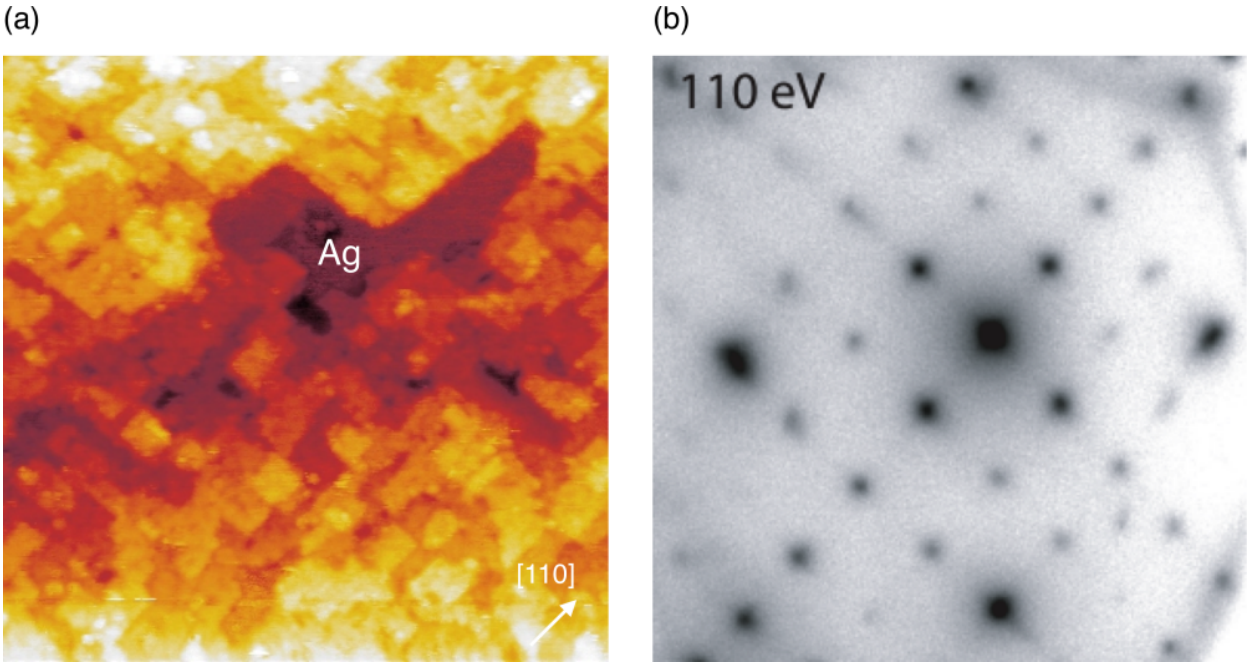

FIG. 7. STM image and LEED pattern of 28 sublayers of Mn_3O_4 on Ag(110) after annealing to 740 K. The LEED pattern shows the superposition of a p(2 × 1) and c(2 × 2) superstructure. In the STM image, the edges of the Mn_3O_4 islands are oriented along [110] directions. The large, deep holes with flat bottoms are assigned to the bare Ag(001) substrate.

The driving force for the structural transition in the Mn_2O_4 top layer is supposedly a decrease in surface energy. Accompanied with growing expansion and perfection of the c(2 × 2) superstructure the amount of polar-edged p(2 × 1) islands decreases. Consequently, the densities of rotated p(2 × 1) domains and domain walls are expected to decrease. This leads to a lower interface energy for the c(2 × 2) superstructure.

In order to test this assumption, 28 sublayers of Mn_3O_4 have been deposited on Ag(001). The increased thickness of the film allows annealing up to 740 K. Although the film ruptures and a few areas with the bare Ag(001) substrate become visible in STM (Fig. 7b), the brilliance of the diffraction pattern and the small size of the LEED spots indicate that film ordering and perfection of the Mn_3O_4 islands are improved. Along with this, the orientation of island edges along [110] directions is more pronounced in the STM image compared to lower coverages. Despite the high film thickness and the large annealing temperature, the LEED pattern does not only show the expected c(2 × 2) superstructure, but the p(2 × 1) superstructure is still present (Fig. 7b). Obviously, the energy difference between the

p(2×1) and c(2×2) superstructures is small even at high coverages of Mn_3O_4. Therefore, the larger entropy favors the simultaneous presence of two superstructures. To understand the mechanisms that lead to the coexistence of p(2×1) and c(2×2) structures even at thick Mn_3O_4 films, we are looking forward to some theoretical descriptions.

IV. CONCLUSIONS

The growth of ultrathin $Mn_3O_4(001)$ films on Ag(001) has been investigated from initial stages up to coverages of 28 sublayers (3.5 unit cells) by a combination of near-edge X-ray absorption fine structure spectroscopy, scanning tunneling microscopy, and low energy electron diffraction. For the initial stages the Mn_3O_4 islands exhibit p(2×1) as well as p(2×2) superstructures with island edges aligned along the [110] directions. For increased film thickness up to 12 sublayers, Mn_3O_4 islands grow embedded into the silver substrate having a p(2×1) superstructures only. Further increase of the film thickness leads to a structural transition of the Mn_3O_4 film with a dominating c(2×2) superstructure next to the p(2×1) superstructure.

ACKNOWLEDGMENTS

Financial support from SFB 762, "Functionality of Oxide Interfaces" is gratefully acknowledged. The authors acknowledge the mutual technical support within the SFB and the beamline staff at BESSY II, Berlin. Particular thanks goes to R. Kulla for technical assistance as well as the scientific discussions in the SFB.

---

[1] H. Hannemann, C. A. J. Ventrice, T. Bertrams, A. Brodde, and H. Neddermeyer, phys. stat. sol. (a) **146**, 289 (1994).

[2] I. Sebastian, M. Heiler, K. Meinel, and H. Neddermeyer, Appl. Phys. A **66**, S525 (1998).

[3] G. A. Rizzi, M. Petukhov, M. Sambi, R. Zanoni, L. Perriello, and G. Granozzi, Surf. Sci. **482-485**, 1474 (2001).

[4] C. Hagendorf, S. Sachert, B. Bochmann, K. Kostov, and W. Widdra, Phys. Rev. B **77**, 075406 (2008).

[5] S. Sachert, S. Polzin, K. Kostov, and W. Widdra, Phys. Rev. B **81**, 195424 (2010).

[6] Y. Martynova, M. Soldemo, J. Weissenrieder, S. Sachert, S. Polzin, W. Widdra, S. Shaikhutdinov, and H. J. Freund, Catal. Lett. **143**, 1108 (2013).

[7] F. Allegretti, C. Franchini, V. Bayer, M. Leitner, G. Parteder, B. Xu, A. Fleming, M. G. Ramsey, R. Podloucky, S. Surnev, and F. P. Netzer, Phys. Rev. B **75**, 224120 (2007).

[8] C. Franchini, R. Podloucky, F. Allegretti, F. Li, G. Parteder, S. Surnev, and F. P. Netzer, Phys. Rev. B **79**, 035420 (2009).

[9] C. Franchini, J. Zabloudil, R. Podloucky, F. Allegretti, F. Li, S. Surnev, and F. P. Netzer, J. Chem. Phys. **130**, 124707 (2009).

[10] F. Li, G. Parteder, F. Allegretti, C. Franchini, R. Podloucky, S. Surnev, and F. P. Netzer, J. Phys. Cond. Mat. **21**, 134008 (2009).

[11] H. Nishimura, T. Tashiro, T. Fujitani, and J. Nakamura, J. Vac. Sci. Technol. **18**, 1460 (2000).

[12] L. Zhang, Z. Tang, S. Wang, D. Ding, M. Chen, and H. Wan, Surface Science **606**, 1507 (2012).

[13] F. Müller, R. de Masi, D. Reinicke, P. Steiner, S. Hüfner, and K. Stöwe, Surf. Sci. **520**, 158 (2002).

[14] M. Nagel, I. Biswas, H. Peisert, and T. Chassé, Surf. Sci. **601**, 4484 (2007).

[15] M. Nagel, I. Biswas, P. Nagel, E. Pellegrin, S. Schuppler, H. Peisert, and T. Chassé, Phys. Rev. B **75**, 195426 (2007).

[16] A. Chassé, C. Langheinrich, F. Müller, and S. Hüfner, Surf. Sci. **602**, 597 (2008).

[17] E. A. Soares, R. Paniago, V. E. de Carvalho, E. L. Lopes, G. J. P. Abreu, and H. D. Pfannes, Phys. Rev. B **73**, 035419 (2005).

[18] O. Y. Gorbenko, I. E. Graboy, V. A. Amelichev, A. A. Bosak, A. Kaul, B. Güttler, V. L. Svetchnikov, and H. W. Zandbergen, Solid State Commun. **124**, 15 (2002).

[19] V. Bayer, R. Podloucky, C. Franchini, F. Allegretti, B. Xu, G. Parteder, M. Ramsey, S. Surnev, and F. Netzer, Phys. Rev. B **76**, 165428 (2007).

[20] K. Takayanagi, K. Yagi, and G. Honjo, Thin Solid Films **48**, 137 (1978).

[21] M. Pivetta, F. Patthey, M. Stengel, A. Baldereschi, and W.-D. Schneider, Phys. Rev. B **72**, 1115404 (2005).

[22] K. Marre and H. Neddermeyer, Surf. Sci. **287/288**, 995 (1993).

[23] K. J. S. Sawhney, F. Senf, M. Scheer, F. Schäfers, J. Bahrdt, A. Gaupp, and W. Gudat, Nucl. Instr. Meth. A **390**, 395 (1997)

[24] A. Chassé, C. Langheinrich, M. Nagel, and T. Chassé, Surf. Sci. **605**, 272 (2011).

[25] B. Gilbert, B. H. Frazer, A. Belz, P. G. Conrad, K. H. Nealson, D. Haskel, J. C. Lang, G. Srajer, and G. D. Stasio, J. Phys. Chem. A **107**, 2839 (2003).

[26] L. Laffont and P. Gibot, Mater. Charact. **61**, 1268 (2010).

[27] P.-T. Chen, C.-M. Tseng, T.-Y. Yung, M.-W. Chu, C.-H. Chen, and M. Hayashi, Ultramicroscopy **140**, 51 (2014).

[28] S. H. Kim, B. J. Choi, G. H. Lee, S. J. Oh, B. Kim, H. C. Choi, J. Park, and Y. Chang, J. Kor. Phys. Soc. **46**, 941 (2005).

[29] J. B. Goodenough and A. L. Loeb, Phys. Rev. **98**, 391 (1955).

[30] K. P. Sinha and A. P. B. Sinha, J. Phys. Chem. **61**, 758 (1957).

[31] K.-M. Schindler, J. Wang, A. Chasse, H. Nedderemeyer, and W. Widdra, Surf. Sci. **603**, 2658 (2009).

[32] Both superstructures are given with respect to the Ag substrate.

[33] R. Shantyr, C. Hagendorf, and H. Neddermeyer, *Proceedings of the 7th International Symposium on Atomically Controlled Surfaces, Interfaces and Nanostructures*, Thin Solid Films **464-465**, 65 (2004).

[34] I. Sebastian, T. Bertrams, K. Meinel, and H. Neddermeyer, Faraday Discuss. **114**, 129 (1999).

[35] A. Ferrari, S. Casassa, C. Pisani, S. Altieri, A. Rota, and S. Valeri, Surf. Sci. **588**, 160 (2005).